NANO LETTERS

Letter

pubs.acs.org/NanoLett

Label-Free Ultrasensitive Memristive Aptasensor

Ioulia Tzouvadaki,*[,†] Pawan Jolly,[‡] Xiaoling Lu,[§] Sven Ingebrandt,[§] Giovanni de Micheli,[†] Pedro Estrela,[‡] and Sandro Carrara[†]

[†]Integrated System Laboratory, École Polytechnique Fédérale de Lausanne, 1015 Lausanne, Switzerland

[‡]Department of Electronic & Electrical Engineering, University of Bath, Bath BA2 7AY, United Kingdom

[§]Department of Informatics and Microsystem Technology, University of Applied Sciences Kaiserslautern, Zweibrücken, Germany

Supporting Information

ABSTRACT: We present the very first worldwide ever-reported electrochemical biosensor based on a memristive effect and DNA aptamers. This novel device is developed to propose a completely new approach in cancer diagnostics. In this study, an affinity-based technique is presented for the detection of the prostate specific antigen (PSA) using DNA aptamers. The hysteretic properties of memristive silicon nanowires functionalized with these DNA aptamers provide a label-free and ultrasensitive biodetection technique. The ultrasensitive detection is hereby demonstrated for PSA with a limit of detection down to 23 aM, best ever published value for electrochemical biosensors in PSA detection. The effect of polyelectrolytes on our memristive devices is also reported to further show how positive or negative charges affect the memristive hysteresis. With such an approach, combining memristive nanowires and aptamers, memristive aptamer-based biosensors can be proposed to detect a wide range of cancer markers with unprecedent ultrasensitivities to also address the issue of an early detection of cancer.

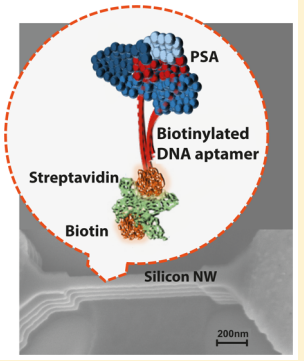

KEYWORDS: *DNA aptamers, biosensors, cancer diagnosis, memristive behavior, silicon nanowires*

Structures like semiconductor nanowires (NWs) show great potential for biosensing applications due to their high surface-to-volume ratio and the possibility of a direct electrical readout. NWs are frequently reported, especially as the channels of field effect transistors in label-free and miniaturized bioassays to detect different biomolecules. On the other hand, several memory effects have been widely reported as appearing in nature[1] as well as in electronic-based devices.[2] A theory for a broad range of systems showing memory effect behavior was developed more than 30 years ago by Chua et al.[3] and very recently reported again by Strukov et al.[4] In these bipolar systems, the memory effect depends upon the charge carriers' rearrangement at the nanoscale level due to external voltage perturbations. Moreover, memory-effect devices have been fabricated using various materials[5,6] and implemented in different applications.[7,8] The present study demonstrates a new application of silicon NW devices that manifest this kind of memory effect: label-free biodetection based on the hysteretic properties of memristive silicon-NW devices functionalized with anti-PSA DNA aptamers, which provide affinity for PSA as a target. PSA is here used as a case study of a prostate cancer biomarker target to demonstrate the applicability of such a new approach for important diagnostics applications, such as early diagnostic of prostate cancer. PSA is a 30 kDa kallikrein protein used as a marker for prostate cancer (PCa); altered levels of PSA in blood above 4 ng/mL (ca. 133 pM) indicate the possibility of prostate cancer and patients are referred to further tests.[9] Such a probe (DNA aptamer)/analyte (PSA) couple was used in order to fabricate ultrasensitive sensors for detection of very low concentration of biomarkers, thus, for the efficient sensing of cancer disease in early stages. DNA aptamers are single stranded DNA sequences that are designed to bind a specific target. More specifically, DNA aptamers are synthetic DNA receptors developed via an in vitro selection technique to bind with high specificity and selectivity to a specific target analyte, like for example a protein, by undergoing a conformational change. DNA aptamers possess many advantages over antibodies such as the possibility for continuous monitoring, enhanced stability, specificity, and reproducibility. All of these characteristics make them as potential candidates to design novel and more specific biosensors.[10]

Results and Discussion. *Surface Characterization.* The surface morphology of the fabricated memristive devices was studied using scanning electron microscopy (SEM) (Figure 1). The SEM micrograph depicts the Si-NW arrays anchored between the NiSi pads, which serve as electrical contacts of the free-standing NW. Schottky-barrier junctions are formed between the Si and NiSi terminals. Due to the top-down nanofabrication process used (see materials and methods section), the width along the structures is not perfectly homogeneous. However, this can increase the freely available area for DNA aptamer binding, which increases DNA aptamer loading and hence better performance of the biosensor.

The Effect of Charged Residues. Before developing the memristive aptasensor, the nanodevices were characterized for

Received: April 22, 2016
Revised: June 16, 2016
Published: June 24, 2016

DOI: 10.1021/acs.nanolett.6b01648
Nano Lett. 2016, 16, 4472−4476

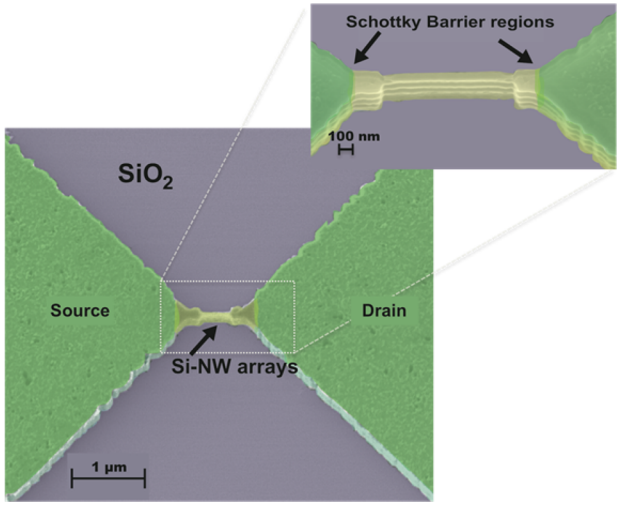

Figure 1. Morphological SEM analysis of Si-NW arrays anchored between NiSi pads.

the effects of charged macromolecules by using a polyelectrolyte (PE) multilayer. PEs are linear macromolecular chains bearing a large number of charged groups when dissolved in a suitable polar solvent. Among them, PSS (poly(sodium 4-styrenesulfonate)) is a strong polyelectrolyte negatively charged in a wide pH range, while PAH (poly(allylamine hydrochloride)) is a weak polyelectrolyte positively charged in neutral or acidic solution or it can be neutral at a pH value above 10.[11] In the case of multilayers of PAH/PSS, each adsorption step leads to a charge inversion on the surface due to the charge overcompensation effect. Subsequent depositions finally result in a PE multilayer stabilized by strong electrostatic forces established among PSS and PAH.[12] The electrical characterization performed on bare nanofabricated wires indicates a hysteretic loop at zero voltage for the forward and the backward curves of the current.[8] In these devices, the memory effect depends on the charge carrier rearrangement at the nanoscale due to external perturbations, such as an applied voltage bias. When charged substances are present on the device surface, the hysteresis is modified, and the current minima for the forward and the backward regimes occur at different voltage values. In this case, a voltage gap is created in the semilogarithmic current−voltage characteristics as a further memory effect on the voltage scan across the nanostructure. The presence of charged substances around the freestanding nanowire creates an electrical field surrounding the channel of the memristive device that controls the channel current.[8] The average voltage gap value after deposition of each layer of PE is shown in Figure 2. Two PE concentrations are implemented, 200 nM and 50 μM. The first electrical measurements are performed after treatment with Piranha solution leading to the appearance of the voltage gap. Afterward, the first PAH adsorption results in narrowing of the voltage gap of 0.09 V difference for 200 nM concentration and 0.16 V difference for the case of 50 μM of PE, respectively. This change is a result of the change in the charge density at the surface of the device due to the positively charged PAH, an effect that is even more pronounced when using an higher concentration of PAH: as more positive charges are present on the surface, a larger voltage gap change is registered. The adsorption of the negatively charged PSS shifts again the average voltage gap to a higher value of 0.17 V, and further treatment with PAH results in a new decrease of the average voltage gap value of 0.15 V for 200 nM concentration of PE. Thus, it is demonstrated that further alternating exchange of the PE solution causes an alternating output signal, which slowly reduces in amplitude. This effect is very similar to the voltage gap trend exhibited in the case of the previously reported antibody−antigen binding.[8] In addition, the consecutive adsorption of the same type of PE (successive adsorption of PSS is presented in Figure 2) tested by implementing the highest concentration of PE results in the acquisition of one direction trend for the voltage gap that increases form the value of 0.05−0.21 V. This one direction trend can be correlated to the increasing voltage gap with the antigen concentration uptake discussed later in this paper.

Analytical Performance. Similarly to what we have observed with PEs, the incorporation of charged biomolecules on the nanostructure produces a change in the voltage gap. The

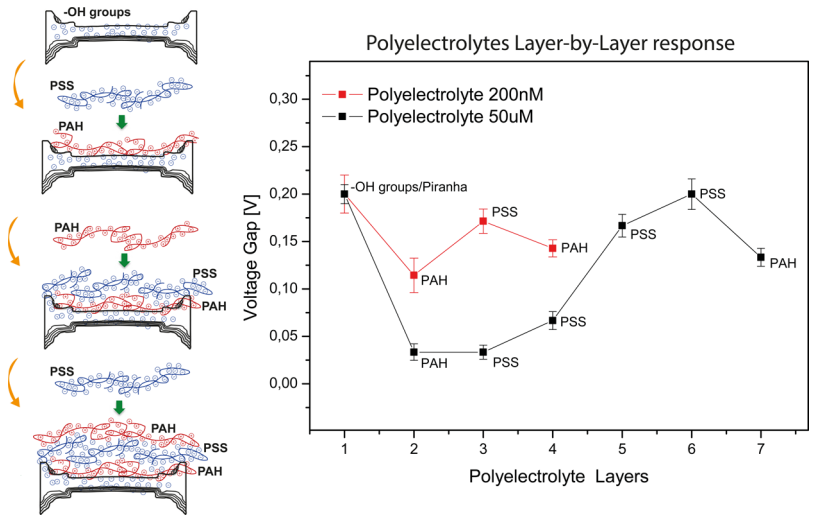

Figure 2. Formation of a multilayer of PEs by repeated electrostatic adsorption of oppositely charged PE layers; average voltage gap value obtained from electrical characterization of devices treated with layer-by-layer deposition of PEs for 200 nM (red points) and 50 μM (black points). The error bars stand for the standard deviation of the voltage gap measured for 14 devices.

DOI: 10.1021/acs.nanolett.6b01648
Nano Lett. 2016, 16, 4472−4476

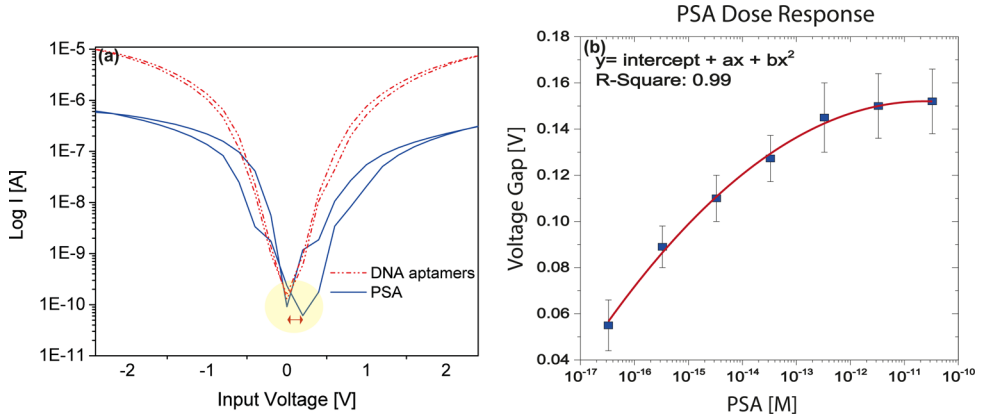

Figure 3. (a) Indicative electrical characteristics demonstrating the introduction of the voltage gap occurring upon biomodification of the surface of the nanodevice. (b) Calibration curve related to the average voltage gap versus dose−response of 10 nanodevices. The reported error bars are the standard deviation of measurements related to these 10 nanodevices.

Table 1. State of the Art List of Reported PSA Electrochemical Aptasensors to Date

method	electrode surface	LOD	reference
quartz crystal microbalance with dissipation mode/electrochemical impedance spectroscopy (EIS)	gold electrodes	37 nM	Formisano et al.[14] (2015)
square wave voltammetry	GCE	pM range	Souada et al.[15] (2015)
EIS	gold electrodes	30 pM	Jolly et al.[16] (2015)
differential pulse voltammetry (DPV)	glassy carbon electrode (GCE)	7.6 pM	Liu et al.[17] (2012)
EIS	GCE	0.15 pM	Kavosi et al.[18] (2015)
EIS	gold electrodes	fM range	Yang et al.[19] (2015)
EIS (capacitance measurement)	gold electrodes	30 fM	Jolly et al.[20] (2016)
DPV	GCE	300 aM	Kavosi et al.[18] (2015)
memristive aptasensor	Si-nanowires	23 aM	present work

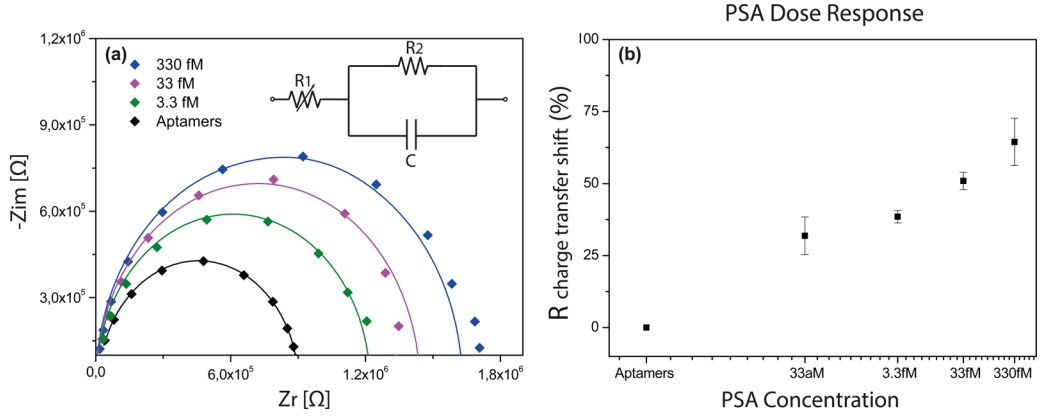

Figure 4. (a) Nyquist plots after DNA aptamer immobilization and after interaction with different concentrations of PSA; the inset shows the Randles circuit used for data fitting. (b) Average dose response charge transfer resistance shift from nine nanofabricated devices. The reported error bars are the standard deviation of measurements related to these nine nanodevices.

presence of biological substances typically contributes to extra charges surrounding the device creating an all-around biogate effect due to the charged groups present in the biomolecules.[8] As a consequence, and in correspondence to the behavior observed in the case of nonbiological molecules, the position of the current minima for the forward and the backward regimes changes introducing a voltage gap in the semilogarithmic current−voltage characteristics as depicted in Figure 3a, which demonstrates an indicative voltage gap opening upon the uptake of 3.3 fM of PSA. The average voltage gap after the biomodification of the device with DNA aptamers and increasing antigen concentration is presented in Figure 3b. A voltage gap of average value of 0.027 V is first obtained for DNA aptamer biomodified NWs, and an increasing trend is acquired with the antigen uptake reaching an average value of 0.152 V for a concentration of 33 pM. On the hand, using a random DNA sequence as control (see Supporting Information), no significant voltage gap difference is observed (<5% difference) even at a high PSA concentration of 33 nM. This demonstrates the specificity and the efficiency of the proposed method. The obtained dose−response for the specific target presented in Figure 3 follows indeed a typical polynomial fit of second-order (quadrant equation) with a root-mean-square value (*R*-Square) of 0.99 and intercept of −0.12 ± 0.04 V. A

DOI: 10.1021/acs.nanolett.6b01648
Nano Lett. 2016, 16, 4472−4476

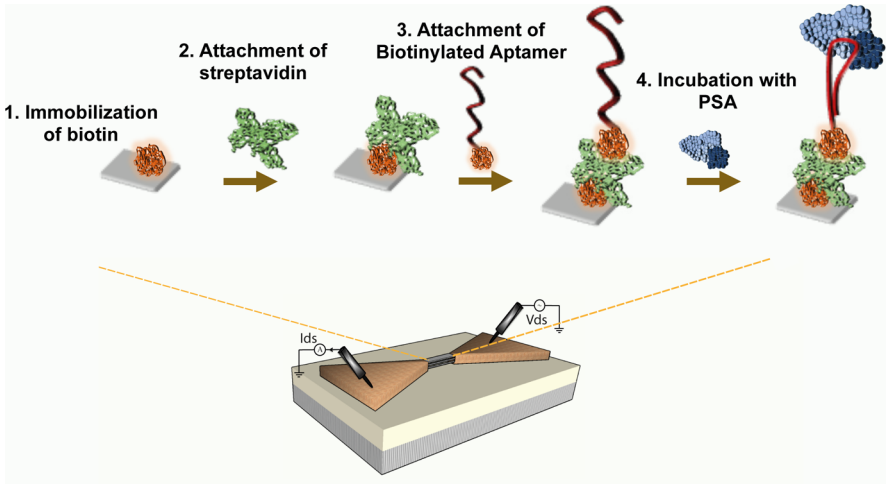

Figure 5. Schematic illustrating the affinity based fabrication process of the memristive aptasensor.

very low limit of detection (LOD) of 23 aM is calculated from 10 independent samples following the method reported by Armbruster et al.[13] The demonstrated LOD is the best ever published so far among electrochemical biosensors for PSA reported in literature (Table 1).

The voltage gap is typically acquired in DC.[8] An AC analysis was also performed in this study for different concentrations of antigen as a complementary characterization. The impedance curves obtained from the electrical characterization of the nanofabricated devices with respect to different antigen concentrations are shown in Figure 4. The device was electrically characterized after the biofunctionalization with DNA aptamers and for four antigen concentrations in the range 33 aM to 330 fM. The corresponding charge transfer resistance values increase from 32% for 33 aM of PSA to 65% for 330 fM. The fact that the charge transfer resistance is increasing with the PSA uptake is coherent with the increased voltage gap registered with increasing PSA uptake. In fact, the large voltage gap may be associated with the larger energy required to move back charge carriers in the NW channel, and this could be attributed to a larger charge transfer resistance. From this standpoint, it can be concluded that the results acquired by AC analysis confirm the outcomes obtained by DC analysis.

Conclusions. In the present work, a novel and definitely innovative aptasensor based on the memristive effect is presented. Memristive properties of silicon nanowires are used to develop an ultrasensitive PSA biosensor based on DNA aptamers. The modification of the related electrical-conductivity hysteresis due to the presence of charged macromolecules was investigated and fully characterized by through the deposition of layer-by-layer polymeric films. The nanofabricated memristive devices were then used to obtain the best ever-fabricated ultrasensitive electrochemical biosensor for the label-free detection of PSA. The demonstrated limit of detection (LOD) of the obtained devices is measured about 23 aM, well below the clinically relevant range of detection for PSA in patient samples. The demonstrated LOD actually is 13 times less with respect the best ever published in the literature so far among many electrochemical biosensors proposed for PSA. Such devices can be easily integrated in LoC (lab-on-a-chip) and PoC (point-of-care) devices for cancer diagnostics, it is fully compatible with standard silicon technology and can easily address the issue of an early detection of cancer thank to the possibility to detect extremely small traces of cancer markers.

Materials and Methods. *Materials.* Biotin (≥99% (TLC), lyophilized powder (B4501)), streptavidin (Streptomyces avidini (S4762)), biotinylated DNA aptamer (5′-[biotin tag] TTT TTA ATT AAA GCT CGC CAT CAA ATA GCT TT-3′), PSS, and PAH were received in powder form (M_w = 70 000 Da) are all purchased from Sigma-Aldrich. PSA (Millipore Angebot R-1939458.1; 539834) was purchased from Merck. The piranha solution was prepared as a mixture of H_2O_2:H_2SO_4 in a 1:2 ratio. Ten mM phosphate buffered saline (PBS) pH 7.4 was filtered through a syringe filter with 0.22 μm pore size, and phosphate buffer (PB) was prepared as 10 mM solution of pH 5.5.

Surface Modification. Memristive Si-NW devices were obtained through a top-down nanofabrication process as described by Tzouvadaki et al.[21] The device surface was treated with piranha solution for 15 min at 70 °C as a cleaning and −OH activation step. The formation of PE multilayers was based on the consecutive adsorption of polyions with alternating charge using the layer-by-layer (LBL) technique as described by Chen and McCarthy.[22] The PE multilayer was formed by consecutive alternate adsorption of positively charged PAH and negatively charged PSS prepared PE solutions (concentrations of 50 μM and 200 nM prepared in PB) and realized by alternately incubation of Si-NW structures for 20 min at room temperature (RT). For the biological sensing the nanodevices were first subjected to 200 μg/mL biotin dissolved in PBS for 2 h at RT and then to 100 μg/mL streptavidin in PBS for another 2 h at RT in dark. Finally, the substrate was incubated overnight in 2 μM of biotinylated anti-PSA DNA aptamer solution in PBS at 4 °C in a humidity chamber. Prior to use, biotinylated DNA aptamers were activated at 95 °C for 10 min before being gradually cooled to room temperature for 30 min.[23] The fabricated memristive aptasensors were investigated for their analytical performance by using PSA at different concentrations in the range of [aM-pM] via consecutive 1 h incubations. Figure 5 illustrates the biofunctionalization steps of the surface, as well as the antigen uptake. After all incubation steps the substrates were washed trice with the corresponding buffer solution and dried in a N_2 flow.

Electrical Characterization Methodology. The electrical characteristics of the nanofabricated memristive structures of

DOI: 10.1021/acs.nanolett.6b01648
Nano Lett. 2016, 16, 4472−4476

mean width of 90 nm and length of 980 nm were acquired using a probe station and contact probes configuration in the semilogarithmic scale using a Keithley 4200SCS semiconductor characterization system from Tektronix GmbH in a two terminal configuration with source measurement unit (SMU), by double sweeping the source to drain voltage between −2.4 V and +2.4 V at a fixed 0 V back-gate potential. These measurements allow the observation of the changing hysteresis properties of the memristive sensors as a function of the surface treatment that leads to a charge variation. The hysteresis was studied in terms of voltage gap calculated between the forward and backward current minima of the I_{ds}−V_{ds} curves. All of the measurements were carried out at RT under a stable humidity environment. Impedance data was acquired using Ivium technologies CompactStat in the frequency range of [1−1000 Hz], amplitude of 1 V in a bias potential of 2.4 V.

SEM Analysis. SEM analysis of the nanofabricated structures was carried out using a scanning electron microscope Merlin from Zeiss. Si-NW arrays configurations were defined using e-beam lithography masks. Imaging performed for 2 kV and stage at 19.5° (main image Figure 1), 15 kV and stage at 34.9° (inset image Figure 1).

■ ASSOCIATED CONTENT

Supporting Information

The Supporting Information is available free of charge on the ACS Publications website at DOI: 10.1021/acs.nanolett.6b01648.

Results obtained with the control sample (PDF)

■ AUTHOR INFORMATION

Corresponding Author

*E-mail: ioulia.tzouvadaki@epfl.ch. Phone: +41 21 69 34243.

Author Contributions

I.T. and P.J. contributed equally. I.T. and P.J. performed sensor fabrication, experiments, and preparation of manuscript. X.L. helped with impedance measurements and analysis and PE solutions preparation. The work was supervised by S.I., P.E., G.d.M., and S.C. The paper was written by I.T. and P.J. and revised by S.I., P.E., G.d.M., and S.C.

Notes

The authors declare no competing financial interest.

■ ACKNOWLEDGMENTS

The authors gratefully acknowledge the staff of the CMI Clean Room of EPFL and M. Zervas for technical advice and fruitful discussions regarding the nanofabrication process. The authors acknowledge financial support from the European Commission FP7 Programme through the Marie Curie Initial Training Network "PROSENSE" (Grant No. 317420, 2012−2016).

■ REFERENCES

(1) Lehn, J.-M. *Chem. Soc. Rev.* **2007**, *36* (2), 151−160.
(2) Wu, J.; McCreery, R. L. *J. Electrochem. Soc.* **2009**, *156* (1), P29−P37.
(3) Chua, L. O.; Kang, S. M. *Proc. IEEE* **1977**, *65* (6), 915−929.
(4) Strukov, D. B.; Snider, G. S.; Stewart, D. R.; Williams, R. S. *Nature (London, U. K.)* **2008**, *453* (7191), 80−83.
(5) Berzina, T.; Smerieri, A.; Bernabò, M.; Pucci, A.; Ruggeri, G.; Erokhin, V.; Fontana, M. *J. Appl. Phys.* **2009**, *105* (12), 124515.
(6) Son, D. I.; Kim, T. W.; Shim, J. H.; Jung, J. H.; Lee, D. U.; Lee, J. M.; Park, W. I.; Choi, W. K. *Nano Lett.* **2010**, *10* (7), 2441−2447.
(7) Sacchetto, D.; Gaillardon, P.-E.; Zervas, M. N.; Carrara, S.; De Micheli, G.; Leblebici, Y. *IEEE Circuits Syst. Mag.* **2013**, *13* (2), 23−41.
(8) Carrara, S.; Sacchetto, D.; Doucey, M.-A.; Baj-Rossi, C.; De Micheli, G.; Leblebici, Y. *Sens. Actuators, B* **2012**, *171*, 449−457.
(9) Catalona, W. J.; Smith, D. S.; Ratliff, T. L.; Dodds, K. M.; Coplen, D. E.; Yuan, J. J.; Petros, J. A.; Andriole, G. L. *N. Engl. J. Med.* **1991**, *324* (17), 1156−1161.
(10) Jolly, P.; Formisano, N.; Estrela, P. *Chem. Pap. - Chem. Zvesti.* **2015**, *69* (1), 77−89.
(11) Mauser, T.; Déjugnat, C.; Sukhorukov, G. B. *Macromol. Rapid Commun.* **2004**, *25* (20), 1781−1785.
(12) Riegler, H.; Essler, F. *Langmuir* **2002**, *18* (17), 6694−6698.
(13) Armbruster, D. A.; Tillman, M. D.; Hubbs, L. M. *Clin. Chem.* **1994**, *40* (7), 1233−1238.
(14) Formisano, N.; Jolly, P.; Bhalla, N.; Cromhout, M.; Flanagan, S. P.; Fogel, R.; Limson, J. L.; Estrela, P. *Sens. Actuators, B* **2015**, *220*, 369−375.
(15) Souada, M.; Piro, B.; Reisberg, S.; Anquetin, G.; Noël, V.; Pham, M. C. *Biosens. Bioelectron.* **2015**, *68*, 49−54.
(16) Jolly, P.; Formisano, N.; Tkáč, J.; Kasák, P.; Frost, C. G.; Estrela, P. *Sens. Actuators, B* **2015**, *209*, 306−312.
(17) Liu, B.; Lu, L.; Hua, E.; Jiang, S.; Xie, G. *Microchim. Acta* **2012**, *178*, 163−170.
(18) Kavosi, B.; Salimi, A.; Hallaj, R.; Moradi, F. *Biosens. Bioelectron.* **2015**, *74*, 915−923.
(19) Yang, Z.; d'Auriac, M. A.; Goggins, S.; Kasprzyk-Hordern, B.; Thomas, K. V.; Frost, C. G.; Estrela, P. *Analyst (Cambridge, U. K.)* **2015**, *140*, 2628−2633.
(20) Jolly, P.; Tamboli, V.; Harniman, R. L.; Estrela, P.; Allender, C. J.; Bowen, J. L. *Biosens. Bioelectron.* **2016**, *75*, 188−195.
(21) Tzouvadaki, I.; Parrozzani, C.; Gallotta, A.; De Micheli, G.; Carrara, S. *J. Bionanosci.* **2015**, *5* (4), 189−195.
(22) Chen, W.; McCarthy, T. J. *Macromolecules* **1997**, *30* (1), 78−86.
(23) Savory, N.; Abe, K.; Sode, K.; Ikebukuro, K. *Biosens. Bioelectron.* **2010**, *26* (4), 1386−1391.

DOI: 10.1021/acs.nanolett.6b01648
Nano Lett. 2016, 16, 4472−4476